Synthesis, Characterization, Thermal Decomposition Mechanism and Non-Isothermal Kinetics of the Pyruvic Acid-Salicylhydrazone and Its Complex of Praseodymium(III)

HE, Shui-Yang*(何水样) LIU, Yu(刘煜) ZHAO, Jian-She(赵建社) ZHAO, Hong-An(赵宏安) YANG, Rui(杨锐) HU, Rong-Zu(胡荣祖) SHI, Qi-Zhen(史启祯)

Shaanxi Key Laboratory of Physico-Inorganic Chemistry & Department of Chemistry, Northwest University, Xi'an, Shaanxi 710069, China

The pyruvic acid-salicylhydrazone and its new complex of Pr(III) were synthesized. The formulae $C_{10}H_{10}N_2O_4$ (mark as H_3L) and $[Pr_2(L)_2(H_2O)_2]\cdot 3H_2O$ (L = the triad form of the pyruvic acid-salicylhydrazone $[C_{10}H_7N_2O_4]^{3-}$) were determined by elemental and EDTA volumetric analysis. Molar conductance, IR, UV, X-ray and ^{1}H NMR were carried out for the characterizations of the complex and the ligand. The thermal decompositions of the ligand and the complex with the kinetic study were carried out by non-isothermal thermogravimetry. The Kissinger's method and Ozawa's method are used to calculate the activation energy value of the main step decomposition. The stages of the decompositions were identified by TG-DTG-DSC curve. The non-isothermal kinetic data were analyzed by means of integral and differential methods. The possible reaction mechanism and the kinetic equation were investigated by comparing the kinetic parameters.

Keywords pyruvic acid-salicylhydrazone, praseodymium(III) complex, thermal decomposition, non-isothermal kinetics, mechanism function

Introduction

Hydrazones act as herbicides, insecticides, nematocides, rodenticides and plant growth regulators. They show spasmolytic activity, hypotensive action and activity against leukaemia, sarcomas and other malignant neoplasm.[1] Rare earth elements have strong biological effect and many complexes of rare earths have all kind of medicinal activities.[2] A series of 2-oxopropionyl(pyridine-4-fomyl)hydrazone with rare earths complexes was synthesized by Yang and the Eu complex showed a certain anticancer activity.[3] There are three radicals in the pyruvic acid-salicylhydrazone that can participate in coordination, that is, the carboxyl group, imide group and the carbonyl group of the amine. Therefore two stable five-numbered circles can be formed. Hence, we think the ligand has a strong ability for coordination and can form stable complexes. It also can be inferred that the complex of pyruvic-acid-salicylhydrazone with Pr(III) has a certain antibiotic activity and agricultural application. TG-DTG-DSC curves can measure the stability, the thermal decomposition mechanism and non-isothermal kinetics of the ligand and the complex, which can furnish useful information for future use.

Experimental

Main reagents

Pyriuvic acid was a biochemical reagent and $Pr(NO_3)_3\cdot 3H_2O$ was prepared in our laboratory. All other chemicals were of A. R. grade.

Analysis methods and main apparatus

The praseodymium(III) of the complex was determined by EDTA volumetric analysis. The C, H and N contents were measured by a PE 2400 elemental analyzer. Molar conductance measurement was made with a DDS-307 conductivity meter. IR spectra were recorded with an EQUINOX55 IR spectrophotometer using sodium chloride disks. UV spectrum was obtained by a Lambda 40 P UV-vis spectrophotometer. ^{1}H NMR spectra were obtained by an INOVA-400-NMR spectrometer. TG-DTG-DSC curves were obtained with a NETZSCH STA 449C thermal analyzer, with Al_2O_3 as a reference at heating rates of 5, 10 and 15 $K\cdot min^{-1}$ in a flowing nitrogen atmosphere, and sample mass used is 2.6—6.3 mg.

Preparation of the ligand

Salicyloyl hydrazide was prepared according to the reported method.[4] The ligand (the pyruvic acid-salicylhydrazone) was prepared by following route (Scheme 1).

Pyruvic acid (1.84 mL) was added to the solution of salicyloyl hydrazide (6.09 g) in nonaqueous alcohol (30

* E-mail: xdhsy@263.net
Received May 20, 2002; revised September 26, 2002; accepted October 15, 2002.
Project supported by the Natural Science Foundation of Shaanxi Province (No. 98H010) and State Key Laboratory of Rare Earth Materials Chemistry and Application & Peking University.

mL). The mixture was stirred on a water bath (80 ℃) for 2 h. The precipitate was filtered and recrystallized from alcohol and washed by ether. The white needle crystal which melted and decomposed at 216 ℃ was obtained with a yield of 75%.

Scheme 1

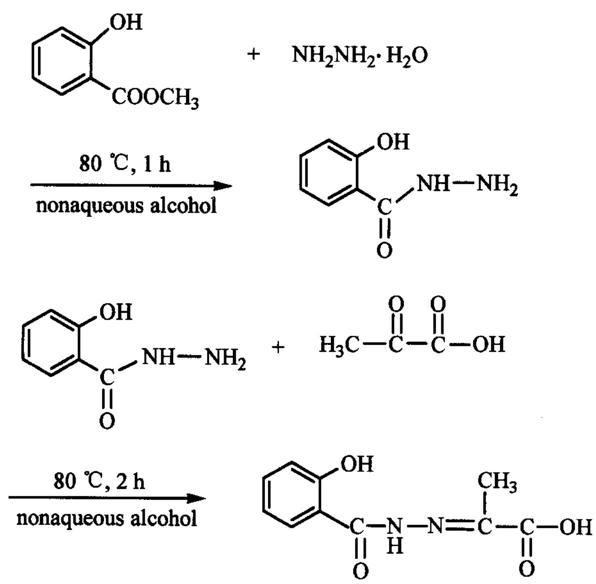

Preparation of the complex

A respective solution of $Pr(NO_3)_3 \cdot 3H_2O$ and the ligand H_3L in nonaqueous alcohol was mixed in 1 : 1 molar ratio. Then triethylamine with three times of the ligand was added. A large quantity of yellow precipitate appeared at once. The mixture was stirred on a water bath (80 ℃) for 4 h. After filtering and washing with alcohol and acetone, the yellow-green powdery complex was obtained with a yield of 95%. The complex was dried in P_4O_{10} desiccator.

Results and discussion

Composition, molar conductance and solubility of the ligand and the complex

The analytical results and molar conductance data at room temperature in DMF for the ligand and the complex are presented in Table 1. The formula $C_{10}H_{10}N_2O_4$ and $[Pr_2(L)_2(H_2O)_2] \cdot 3H_2O$ were analyzed respectively. The ligand is 1 : 1 electrolyte, which indicate that H^+ on carboxyl group in the ligand is free in DMF. The complex is non-electrolyte.[5]

The ligand H_3L is insoluble in ether, sparingly soluble in water and acetone, soluble in methanol and alcohol, and easily soluble in DMF and DMSO. The complex is insoluble in ether and acetone, sparingly soluble in water, methanol and alcohol, and easily soluble in DMF and DMSO.

Spectra study

A. *Infrared spectra*

IR spectra of the ligand and the complex are carried out according to Ref. 6, 7, 8. Some data are quite different between the ligand and the complex, which shows the structure change of the ligand after coordination. The disappearance of $\nu_{C=O}$ (−COOH) (1755 cm^{-1}) in the ligand and the appearance of $\nu_{as}(CO_2^-)$ (1540 cm^{-1}) and $\nu_s(CO_2^-)$ (1460 cm^{-1}) are assigned to the coordination of the carboxyl group. The $\Delta\nu$ ($\nu_{as} - \nu_s$) (80 cm^{-1}) less than the $\Delta\nu_L$(164—171 cm^{-1}) in the sodium and potassium salt suggests a possibility of bridging ligand.[6] The absence of amine I ($\nu_{C=O}$) (1639 cm^{-1}) in the complex points to the coordination of the C = O group. Amine II (δ_{NH}) (1532 cm^{-1}) is absent in the complex too, pointing to the loss of the proton here. Amine III ($\nu_{C—N}$) (1290 cm^{-1}) is shifted to 1340 cm^{-1}, indicating the C—N bond has been strengthened. The absence of δ_{OH} (ArOH) (1383 cm^{-1}) in the complex indicates the loss of hydrogen in ArOH group. The $\nu_{N—N}$ is shifted from 1158 to 1161 cm^{-1} after coordination, which shows that the N—N bond has been strengthened. There is also a new strong and wide band of water (3392 cm^{-1}) in the complex. The bands at 820 cm^{-1} and 520 cm^{-1} indicate that water was coordinated.[7] Therefore it can be inferred that the ligand coordination as a tridentate binding, that is, two five-numbered circles are formed by the amido enol oxygen, imido nitrogen and carboxyl oxygen with Pr(III).

B. UV *Spectra*

UV spectra of the ligand and the complex were obtained in DMF solution with DMF as a reference. The data are listed in Table 2. There is a strong band at 314.52 nm in the ligand, which is the π-π^* transition of the salicyloyl group. Its red shift to 329.50 nm in the complex shows that the conjugation of the salicyloyl group has been strengthened.

Table 1 Composition and molar conductance data of the ligand and the complex

Sample	$b^a \times 10^{-4}$ (mol·L^{-1})	Λ_m (s·cm^2·mol^{-1})	Color	C%	H%	N%	Pr%
Ligand	2.25	45.8	white	53.72 (54.05)	4.68 (4.54)	12.85 (12.61)	—
Complex	9.90	13.7	yellow-green	29.91 (29.65)	3.23 (2.99)	6.96 (6.91)	34.35 (34.79)

[a] *b* is concentration of the ligand and the complex. The data in bracket are calculated values.

Table 2 UV spectra of the ligand and the complex

Sample	$b \times 10^4$ ($mol \cdot L^{-1}$)	λ^a (nm)
Ligand	1.1	314.52
Complex	2.0	329.50

^{a} Absorption wavelength.

C. ^{1}H NMR *spectra*

^{1}H NMR spectra of the ligand and the complex were obtained at room temperature in DMSO solution. The proton labels of the ligand are showed in Fig. 1 and the data of the proton chemical shifts are shown in Table 3. The disappearance of the proton chemical shifts of - COOH, - CONHN = , ArOH in the complex show the loss of the protons after coordination. The changes of the methyl and phenyl group indicate the coordination of the ligand in the complex indirectly. Because of the water in the complex, a new chemical shift of the proton in water appears, too.

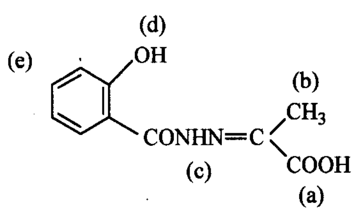

Fig. 1 Labels of the ligand.

Table 3 ^{1}H NMR data of the compounds (10^{-6})

Sample	δ_a	δ_b	δ_c	δ_d	δ_e	δ_{H_2O}
Ligand	13.83	2.13	11.78	11.38	6.93—7.98	—
Complex	—	2.01	—	—	8.66—9.04	3.33

X-*Ray powder diffraction*

The results of the X-ray powder diffraction for the ligand, the salt and the complex respectively are shown in Table 4, indicating that: (1) X-ray powder diffraction of the complex is different from the ligand and the salt obviously; (2) the complex is not simple lap joint of the ligand and the salt either; (3) a new compound is formed.

Thermal behaviors of the complex

A. *Thermal behaviors of the ligand and complex*

The TG-DTG-DSC curves of the ligand and the complex are shown in Fig. 2. The ligand changes into a brown yellow liquid and fiercely decomposes at 216 ℃ on the melting point apparatus. It is also shown that the ligand decomposes rapidly at 167—209—231 ℃ in Fig. 2. The two results fairly agree with each other. The decomposition stages can be inferred as follows (what in the parentheses is theoretical weight lost (%) and ΔH_d is decomposition enthalpy) (Scheme 2).

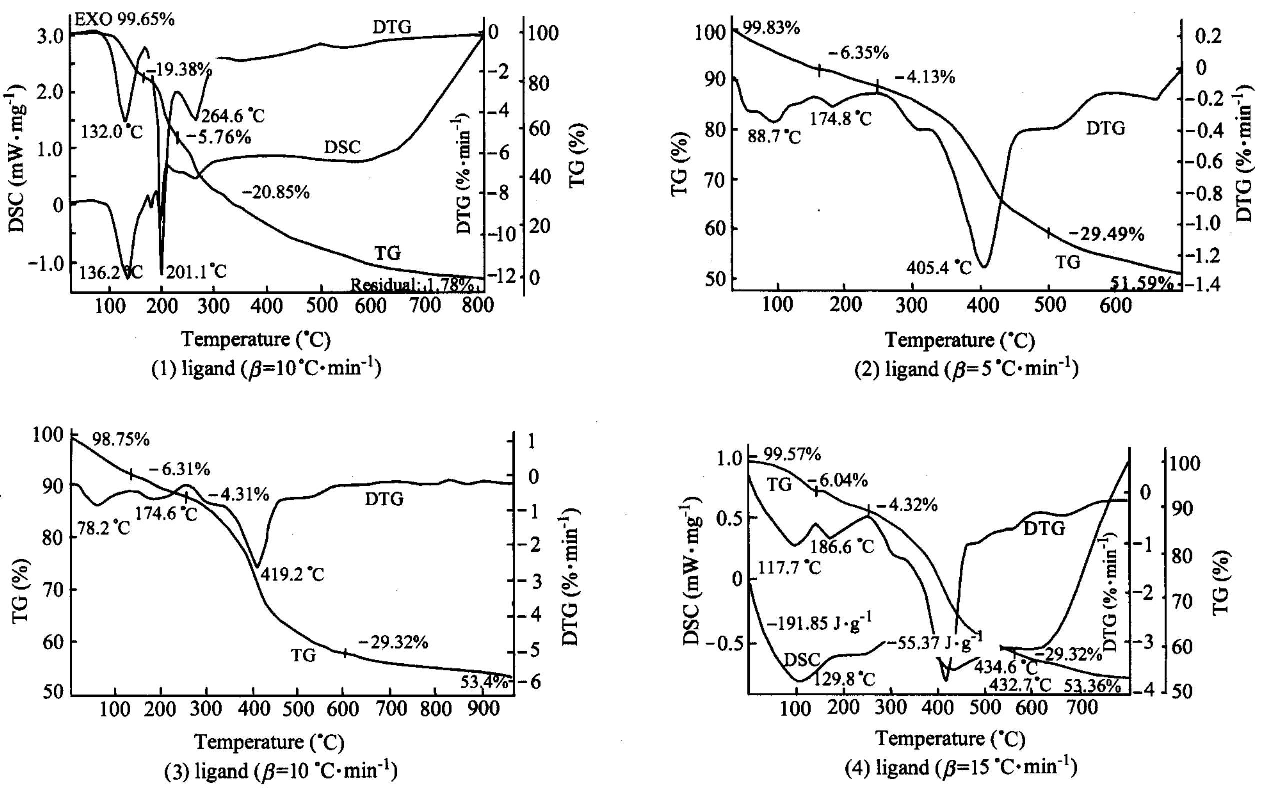

Fig. 2 TG-DTG-DSC curves of the ligand and the complex.

Table 4 Data of X-ray for the ligand, salt and complex

Sample		Main diffraction data							
$Pr(NO_3)_3\cdot$	I/I_0	100	90	85	80	75	70	60	50
$6H_2O$	d (nm)	0.8040	0.6280	0.4480	0.4390	0.2880	0.3920	0.6200	0.2438
Ligand	I/I_0	100	82	73	61	56	55	46	40
	d (nm)	0.3601	0.3386	0.3684	0.5611	0.6321	0.5764	0.6021	0.4691
Complex	I/I_0	100	36	34	25	24	22	21	20
	d (nm)	1.6055	0.4350	1.0493	0.7838	0.3739	0.2346	0.2949	1.4669

Scheme 2

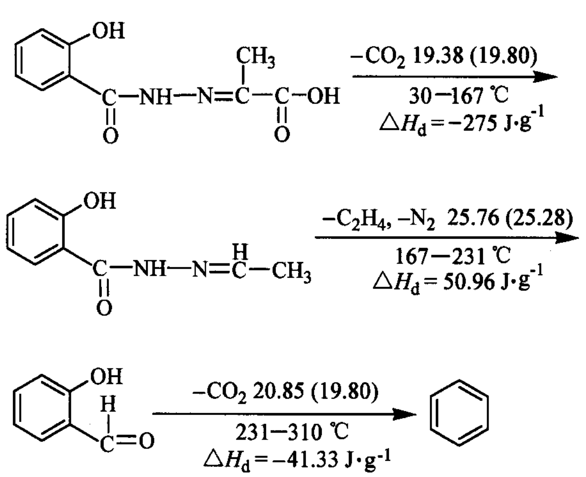

The ligand decomposes completely and has no remainder. The thermal decomposition stages and the ranges of temperature of the complex are listed in Table 5. The thermal decomposition process of the complex can be divided into three stages: the first-stage consists of two steps endothermic dehydration process. The first step is connected with the loss of three molecules of crystal water from the complex and the peak of temperature is 117.7 ℃ ($\beta = 15$ $K\cdot min^{-1}$) on the DTG curve. The second step results in a loss of two hydrous water molecules and the peak temperature is 186.6 ℃ ($\beta = 15$ $K\cdot min^{-1}$). The first-stage mass loss is 10.36% between 30 ℃ and 268 ℃, which coincides with the calculated value (11.12%) of losing five water molecules from the complex. The dehydration enthalpy value (ΔH_d) of the complex in this stage is -191.85 $J\cdot g^{-1}$. Two ($N_2 + C_6H_4O^-$) are lost in the second-stage decomposition process and the peak temperature is 432.7 ℃ ($\beta = 15$ $K\cdot min^{-1}$). The decomposition enthalpy value (ΔH_d) of the complex in this stage is -55.37 $J\cdot g^{-1}$. The third-stage is the further decarburization and dehydrogenation. The remainders are black. By elemental analysis, there is not any H and N, the quantity of the carbon is coincident to the ratio in Table 5. Combining IR, ^1H NMR spectra and the requirement of the common coordination number of rare earth complexes,[9] the possible structure of the complexes is inferred as shown in Fig. 3, that is, the binuclear complex is formed by two Pr(Ⅲ) and the carboxyl oxygen acting as a monatomic bridging atom.[6] The hydrous waters also coordinate with the two Pr(Ⅲ) in a bridging manner in the vertical direction of the plane of the ligand. That makes the coordination number of Pr(Ⅲ) to be six. The mass losses agree with the theoretic value of the corresponding fragments in every stage, which is the further verification of the structure.

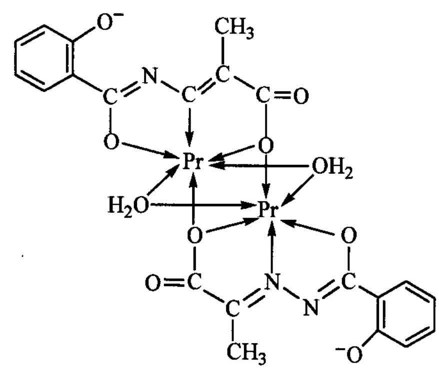

Fig. 3 Structure of the complex.

Table 5 Thermal decomposition stages and the ranges of temperature of the complex

β ($K\cdot min^{-1}$)	The first-stage			The second-stage			Final	
	Piece	Loss of mass (%)	Temp. range (℃)	Piece	Loss of mass (%)	Temp. range (℃)	Remainder	Ratio of remainder (%)
5	$3H_2O$	6.35 (6.67)	30—151	$2(N_2 + C_6H_4O^-)$	29.49	252—493	$1/3(Pr_6O_{11}) + 6C$	51.59
	$2H_2O$	4.13 (4.45)	151—252		(29.65)			(50.92)
10	$3H_2O$	6.31 (6.67)	30—152	$2(N_2 + C_6H_4O^-)$	29.32	259—533	$1/3(Pr_6O_{11}) + 8C$	53.40
	$2H_2O$	4.31 (4.45)	152—259		(29.65)			(53.88)
15	$3H_2O$	6.04 (6.67)	30—166	$2(N_2 + C_6H_4O^-)$	29.32	268—535	$1/3(Pr_6O_{11}) + 8C$	53.36
	$2H_2O$	4.32 (4.45)	166—268		(29.65)			(53.88)

B. *Non-isothermal decomposition kinetics of the complex*

The data needed for the calculations of the mechanism function and kinetics for the second-stage decomposition of the complex are summarized in Table 6, where α_i is the fraction of the sample reacted. T_i the corresponding reaction temperature, $(dH_t/dt)_i$ the endothermic rate, T_0 the initial point of the deviation from the baseline of the DSC or DTG curve, H_0 the total endothermic of the sample, and β the constant heating rate.

The kinetic parameters and the most possible kinetic mechanism function of the second-stage decomposition process of the complex were obtained by the MacCallum-Tanner equation (1)[10], the differential equation (2)[11] and the method of comparing the kinetic parameters.

$$\lg G(\alpha) = \lg(AE/\beta R) - 0.4828E^{0.4358} - (0.449 + 0.217E)/0.001T \quad (1)$$

$$\ln\{(d\alpha/dT)\{f(\alpha)[E(T-T_0)/RT^2+1]\}\} = \ln[A/\beta] - E/RT \quad (2)$$

where A is the pre-exponential factor, E the activation energy, $f(\alpha)$ the differential mechanism function, $G(\alpha)$ the integral mechanism function. By substituting the forty-one types of kinetic mechanism functions in Table 7 and data in Table 6 into Eqs. (1) and (2), the values of E, lg A, the linear correlation coefficient (r) and standard deviation (SD) tabulated in Table 8 are obtained by the method of logical choices, indicating that the second-stage decomposition of the complex is classified as random nucleation and subsequent growth, and the most probable kinetic mechanism function is No. 18, the Avrami-Erofeer equation with $n = 2$, heating rate has a little influence on the kinetic parameters. The average value of E of the second-stage decomposition reaction is 148.8 $kJ\cdot mol^{-1}$. The average of A is $10^{8.91}$ s^{-1}. These values of E and A are in agreement with the calculated values obtained by the methods of Kissinger[12] and Ozawa[13] shown in Table 9.

Substituting $f(\alpha)$ with $1/2(1-\alpha)[-\ln(1-\alpha)]^{-1}$, E with 149.6 $kJ\cdot mol^{-1}$, β with 5 $K\cdot min^{-1}$ and A with $10^{9.05}$ s^{-1} in Eq. (2), we can now establish the kinetics equation of the second-stage decomposition of the complex as follows [Eq. (3)]:

$$d\alpha/dT = 10^{9.05}(1-\alpha)[-\ln(1-\alpha)]^{-1}[1 + 17994(T-T_0)/T^2]\exp(-17994/T) \quad (3)$$

Table 6 Base data of the second-stage decomposition of the complex

Data point	$\beta = 15$ $K\cdot min^{-1}$ [a]			$\beta = 10$ $K\cdot min^{-1}$		$\beta = 5$ $K\cdot min^{-1}$	
	T_i (℃)	α_i	$(dH_t/dt)_i$ $(mW\cdot mg^{-1})$	T_i (℃)	α_i	T_i (℃)	α_i
1	361.5	0.2273	-0.5268	361.3	0.2608	361.3	0.2884
2	366.5	0.2459	-0.5284	366.3	0.2794	366.3	0.3139
3	371.5	0.2646	-0.5303	371.3	0.3001	371.3	0.3429
4	376.5	0.2853	-0.5292	376.3	0.3205	376.3	0.3753
5	381.5	0.3070	-0.5336	381.3	0.3429	381.3	0.4088
6	386.5	0.3305	-0.5381	386.3	0.3694	386.3	0.4460
7	391.5	0.3546	-0.5473	391.3	0.3974	391.3	0.4833
8	396.5	0.3819	-0.5620	396.3	0.4288	396.3	0.5257
9	401.5	0.4115	-0.5746	401.3	0.4629	401.3	0.5695
10	406.5	0.4453	-0.5865	406.3	0.4998	406.3	0.6154
11	411.5	0.4819	-0.6055	411.3	0.5426	411.3	0.6616
12	416.5	0.5212	-0.6351	416.3	0.5830	416.3	0.7037
13	421.5	0.5623	-0.6654	421.3	0.6285	421.3	0.7430
14	426.5	0.6061	-0.6896	426.3	0.6678	426.3	0.7785
15	431.5	0.6495	-0.7060	431.3	0.7078	431.3	0.8068
16	436.5	0.6920	-0.7188	436.3	0.7430	436.3	0.8310
17	441.5	0.7309	-0.7217	441.3	0.7716	441.3	0.8506
18	446.5	0.7644	-0.7218	446.3	0.7937	446.3	0.8679
19				451.3	0.8123	451.3	0.8841
20				456.3	0.8279	456.3	0.8986

[a] $T_0 = 30$ ℃, $H_0 = 55.37$ $J\cdot g^{-1}$.

Table 7 Common mechanism functions $f(\alpha)$ and $G(\alpha)$ in non-isothermal reaction kinetics

No.	Name of function	$f(\alpha)$	$G(\alpha)$	Mechanism
1	Parabola law	$\alpha^{-1}/2$	α^2	one-dimensional diffusion, 1D
2	Valensi equation	$[-\ln(1-\alpha)]^{-1}$	$\alpha+(1-\alpha)\ln(1-\alpha)$	two-dimensional diffusion, 2D
3	Jander equation	$4(1-\alpha)^{1/2}[1-(1-\alpha)^{1/2}]^{1/2}$	$[1-(1-\alpha)^{1/2}]^{1/2}$	two-dimensional diffusion, 2D, $n=1/2$
4	Jander equation	$(1-\alpha)^{1/2}[1-(1-\alpha)^{1/2}]^{-1}$	$[1-(1-\alpha)^{1/2}]^{2\alpha}$	two-dimensional diffusion, 2D, $n=2$
5	Jander equation	$6(1-\alpha)^{2/3}[1-(1-\alpha)^{1/3}]^{1/2}$	$[1-(1-\alpha)^{1/3}]^{1/2}$	three-dimensional diffusion, 3D, $n=1/2$
6	Jander equation	$3(1-\alpha)^{2/3}[1-(1-\alpha)^{1/3}]^{-1}/2$	$[1-(1-\alpha)^{1/3}]^2$	three-dimensional diffusion, spheres symmetry, 3D, $n=2$
7	G.-B. equation[a]	$3[(1-\alpha)^{-1/3}-1]^{-1}/2$	$1-2\alpha/3-(1-\alpha)^{2/3}$	three-dimensional diffusion, 3D
8	Anti-Jander equation	$3(1+\alpha)^{2/3}[(1+\alpha)^{1/3}-1]^{-1}/2$	$[(1+\alpha)-1]^2$	three-dimensional diffusien, 3D
9	Z.-L.-T. equation[b]	$3(1-\alpha)^{4/3}[(1-\alpha)^{1/3}-1]^{-1}/2$	$[(1-\alpha)^{-1/3}-1]^2$	three-dimensional diffusion, 3D
10	Avrami-Erofeev equation	$4(1-\alpha)[-\ln(1-\alpha)]^{3/4}$	$[-\ln(1-\alpha)]^{1/4}$	assumes random nucleation and its subsequent growth, $n=1/4$, $m=4$
11	Avrami-Erofeev equation	$3(1-\alpha)[-\ln(1-\alpha)]^{2/3}$	$[-\ln(1-\alpha)]^{1/3}$	(same as above) $n=1/3$, $m=3$
12	Avrami-Erofeev equation	$5(1-\alpha)[-\ln(1-\alpha)]^{2/5}/2$	$[-\ln(1-\alpha)]^{2/5}$	(same as above) $n=2/5$
13	Avrami-Erofeev equation	$2(1-\alpha)[-\ln(1-\alpha)]^{1/2}$	$[-\ln(1-\alpha)]^{1/2}$	(same as above) $n=1/2$, $m=2$
14	Avrami-Erofeev equation	$3(1-\alpha)[-\ln(1-\alpha)]^{1/3}/2$	$[-\ln(1-\alpha)]^{2/3}$	(same as above) $n=2/3$
15	Avrami-Erofeev equation	$4(1-\alpha)[-\ln(1-\alpha)]^{1/4}/3$	$[-\ln(1-\alpha)]^{3/4}$	(same as above) $n=3/4$
16	Avrami-Erofeev equation	$1-\alpha$	$-\ln(1-\alpha)$	(same as above) $n=1$, $m=1$
17	Avrami-Erofeev equation	$2(1-\alpha)[-\ln(1-\alpha)]^{-1/2}/3$	$-\ln(1-\alpha)$	(same as above) $n=3/2$
18	Avrami-Erofeev equation	$(1-\alpha)[-\ln(1-\alpha)]^{-1}/2$	$[-\ln(1-\alpha)]^2$	(same as above) $n=2$
19	Avrami-Erofeev equation	$(1-\alpha)[-\ln(1-\alpha)]^{-2}/3$	$[-\ln(1-\alpha)]^3$	(same as above) $n=3$
20	Avrami-Erofeev equation	$(1-\alpha)[-\ln(1-\alpha)]^{-3}/4$	$[-\ln(1-\alpha)]^4$	(same as above) $n=4$
21	P.-T. equation[c]	$\alpha(1-\alpha)$	$\ln[\alpha/(1-\alpha)]$	auto catalysis, branch random nucleation
22	Mampel power law	$4\alpha^{3/4}$	$\alpha^{1/4}$	$n=1/4$
23	Mampel power law	$3\alpha^{2/3}$	$\alpha^{1/3}$	$n=1/3$
24	Mampel power law	$2\alpha^{1/2}$	$\alpha^{1/2}$	$n=1/2$
25	Mampel power law	1	α	phase boundary reaction, R_1, $n=1$
26	Mampel power law	$2\alpha^{-1/2}/3$	$\alpha^{3/2}$	$n=3/2$
27	Mampel power law	$\alpha^{-1}/2$	α^2	$n=2$
28	Reaction order	$4(1-\alpha)^{3/4}$	$1-(1-\alpha)^{1/4}$	$n=1/4$
29	Contracting sphere (volume)	$3(1-\alpha)^{2/3}$	$1-(1-\alpha)^{1/3}$	phase boundary reaction (one-dimension), $n=1/3$,
30		$1-(1-\alpha)^{2/3}$	$3[1-(1-\alpha)^{1/3}]$	$n=3$, (three-dimension)
31	Contracting cylinder (area)	$2(1-\alpha)^{1/2}$	$1-(1-\alpha)^{1/2}$	phase boundary reaction, $n=1/2$,
32		$(1-\alpha)^{1/2}$	$2[1-(1-\alpha)^{1/2}]$	$n=2$, (two-dimension)
33	Reaction order	$(1-\alpha)^{-1}/2$	$1-(1-\alpha)^2$	$n=2$
34	Reaction order	$(1-\alpha)^{-2}/3$	$1-(1-\alpha)^3$	$n=3$
35	Reaction order	$(1-\alpha)^{-3}/4$	$1-(1-\alpha)^4$	$n=4$
36	Second order	$(1-\alpha)^2$	$(1-\alpha)^{-1}$	chemical reaction, F_2
37	Reaction order	$(1-\alpha)^2$	$(1-\alpha)^{-1}-1$	chemical reaction
38	2/3 order	$2(1-\alpha)^{3/2}$	$(1-\alpha)^{-1/2}$	chemical reaction
39	Exponent law	α	$\ln\alpha$	E_1, $n=1$
40	Exponent law	$\alpha/2$	$\ln\alpha^2$	$n=2$
41	Third order	$(1-\alpha)^3/2$	$(1-\alpha)^{-2}$	chemical reaction, F_3

[a] Ginstling-Brounshtein equation. [b] Zhuralev-Lesokin-Tempelman equation. [c] Prout-Tompkins equation.

Table 8 The best kinetic parameter of all kinds of calculation methods

Calculation methods	β (K·min^{-1})	E (kJ·mol^{-1})	lg A (s^{-1})	r	SD	Function No.
MacCallum-Tanner	5	155.3	9.44	0.9978	0.1578	18
	10	145.4	8.72	0.9972	0.1655	18
	15	148.0	8.98	0.9956	0.1838	18
Differential equation	15	146.3	8.51	0.9829	0.7927	18
average		148.8	8.91			

Table 9 Values of E and A of the complex obtained by the Kissinger's method and Ozawa's method[a]

β (K·min^{-1})	T_p (K)	E_a (kJ·mol^{-1})	A (s^{-1})	r_k	E_0 (kJ·mol^{-1})	r_0
15	705.7					
10	692.2	149.6	$10^{9.05}$	0.989	153.2	0.991
5	678.5					

[a] β is the heating rate, T_p the peak temperature of DTG, E_a and E_0 the apparent activation energy obtained by Kissinger's method and Ozawa's method, respectively and A the pre-exponential constant, r_k the linear correlation coefficient.

References

1 Mohan, K. *Talanta* **1975**, *22*, 151.

2 Tang, Z.-X.; Zhang, F.-X.; Wang, J.-M.; Fang, Y. *Medium Inorganic Chemistry*, the Publishing House of Chengdu Science and Technology University, Chengdu, **1993**.

3 Yang, Z.-Y.; Wang, L.-F.; Wu, J.-G. *Chin. J. Appl. Chem.* **1992**, *9*, 31 (in Chinese).

4 Naraneetham, N. S.; Lalyanasundaram, R.; Soundararajan, S. *Inorg. Chim. Acta* **1985**, *110*, 169.

5 Geary, W. J. *Coord. Chem. Rev.* **1971**, *7*, 81.

6 Deacon, G. B.; Philips, R. J. *Coord. Chem. Rev.* **1980**, *33*, 227.

7 Kazuo, N., Translated by Huang, D.-R.; Wang, R.-Q. *Infrared and Raman Spectra of Inorganic and Coordination Compounds*, Chemical Industry Press, Beijing, **1986**, 199.

8 Chen, Y.-Z. *Organic Analysis*, Higher Education Press, Beijing, **1981**.

9 Su, Q. *Rare Earth Chemistry*, Henan Science and Technology Press, Zhengzhou, **1993**.

10 MacCallum, J. R.; Tanner, J. *Eur. Polymer J.* **1968**, *4*, 333.

11 Bagchi, T. P.; Sen, K. P. *Thermochim. Acta* **1981**, *51*, 175.

12 Kissinger, H. E. *Anal. Chem.* **1957**, *29*, 17024.

13 Ozawa, T. *Bull. Chem. Soc. Jpn.* **1965**, *38*, 1881.

(E0205205 ZHAO, X. J.; LING, J.)